Biosensors and Bioelectronics 138 (2019) 111318

Contents lists available at ScienceDirect

Biosensors and Bioelectronics

journal homepage: www.elsevier.com/locate/bios

Novel coreactant modifier-based amplified electrochemiluminescence sensing method for point-of-care diagnostics of galactose

Yixin Nie, Yang Liu, Qian Zhang, Xingguang Su**, Qiang Ma*

Department of Analytical Chemistry, College of Chemistry, Jilin University, Changchun, 130012, China

ARTICLE INFO

Keywords:
N-dots
Electrochemiluminescence
Coreactant modifier
Galactose detection
ECL digital imaging

ABSTRACT

Herein, an innovative coreactant modifier-based amplified ECL sensing method was developed to provide a convenient and effective amplified ECL emission. Firstly, nitrogen-rich quantum dots (N-dots) were prepared. N-dots have much nitrogen functional groups, which provide more reactive sites on the surface in the ECL reaction. Furthermore, we investigated the action mechanism of H_2O_2 as coreactant modifier to promote the generation of more oxidant of coreactant in the N-dot/$K_2S_2O_8$ coreactant ECL pathway. The coreactant modifier can generate ca. 40- and 7.7-times intensity over that of H_2O_2 or $K_2S_2O_8$ as an individual coreactant, respectively. Finally, the proposed biosensor was designed to accurately quantify galactose (GA) from 0.5 μmol L^{-1} to 15 mmol L^{-1} with a limit of detection (LOD) of 0.16 μmol L^{-1}. This coreactant modifier-based amplified ECL sensing method significantly improved the sensitivity and accuracy of enzyme sensors. And it was applied in spiked human serum samples with satisfactory results. Moreover, the change of the ECL signal can be easily imaged and observed with the help of a smartphone camera, which satisfied the needs of point-of-care test of GA.

1. Introduction

The accurate determination of the GA level in human urine is of importance in the fields of food science, human nutrition, fermentation industry and medicine (Tk'c1 et al., 1999; Garcia-Carmona et al., 2016; Taylor et al., 1977). GA is present at a maximum concentration of 0.28 mM in normal adults and 1.11 mM in neonatal infants less than 5 days old (Stoecker et al., 1995). High concentrations GA can result in fatal galactosemia (Lee et al., 2011) and endanger the newborns life. Complications of galactosemia are extremely harmful to health. A small number of patients may have retinal and vitreous hemorrhage, jaundice and hepatic enlargement, cirrhosis, ascites, liver failure, hemorrhage, growth retardation, intelligent development, high chloride acidosis, protein urine, amino aciduria and hypoglycemia. In particular, newborns who are not diagnosed and treated correctly at the early stage will die in the neonatal period, with a 6-week average life. Even if they are spared, they will still have mental retardation in the future. Therefore, a simple and effective way for the point-of-care diagnostics of GA becomes a necessary issue. GA detection tended to be via laser-induced fluorescence (Easley et al., 2003), capillary electrophoresis coupled with electrochemical detection (Manowitz et al., 1995; Brahim et al., 2002), and high-performance liquid chromatography (Nishimura et al., 2004). But these methods relied on large instruments and complex operation with low sensitivity. Therefore, to develop a simple, economical and efficient way for clinical detection of GA is an important issue.

Traditional quantum dots (QDs) (Alivisatos, 1996) consisting of hundreds to thousands of atoms are prominent in the field of optoelectronics (Englund et al., 2005; Larson et al., 2003; Sasaki et al., 2000), and are widely used as sensors of analytical detection for various attractive properties (Zhang et al., 2015), which are successfully applied in bioimaging (Gao et al., 2004; Medintz et al., 2005; Michalet et al., 2005) clinical drug delivery (Zrazhevskiy et al., 2010; Bagalkot et al., 2007). However, the heavy metal elements contained in conventional QDs are not conducive to bioanalysis due to their high toxicity and the environmental damage caused by emissions. Therefore, biocompatible and environmentally friendly QDs have been developed, such as carbon QDs (Sun et al., 2006; Baker and Baker, 2010), graphene QDs (GQDs) (Ponomarenko et al., 2008; Pan et al., 2010), boron QDs (Lin et al., 2014), carbon nitride QDs (Fan et al., 2015; Tang et al., 2013, 2014), silicon QDs (Ding et al., 2002), carbon silicon QDs (Sun et al., 2016). These QDs are highly soluble, less toxic, and particularly biocompatible, with practical application in catalyst (Yeh et al., 2014), photovoltaic devices (Shen et al., 2012), biological and environmental sensors (Zhu et al., 2013) and excellent bioimaging (Cao et al., 2007). Carbon QDs as the most widely used in non-heavy metal QDs exhibit

* Corresponding author.
** Corresponding author.
E-mail address: Qma@jlu.edu.cn (Q. Ma).

https://doi.org/10.1016/j.bios.2019.111318
Received 5 March 2019; Received in revised form 29 April 2019; Accepted 9 May 2019
Available online 10 May 2019
0956-5663/

the merits of non-toxicity, good electrical conductivity and chemical/photo stability. Especially after surface modification and hetero atom doping, functionalized carbon QDs are extensively used as biochemical sensors with broad application prospects. However, deficiencies of their complicated and time-consuming synthesis with high temperature and strong acid treatment limit their application. At present, low content of heteroatoms and non-internal doping undoubtedly make it difficult to study the formation mechanism and obtain satisfactory properties of carbon QDs. Nitrogen doping and co-doping with other heteroatoms are the commonest doping methods for carbon QDs. Compared with C atom, N atom with larger electron atomicity motivates the polarization of conjugated system. The change of original electron cloud density distribution of carbon lattice due to the doping of N atom affects physical and chemical properties of carbon QDs. N-dots with much higher nitrogen content than that in nitrogen-doped carbon QDs can significantly increase the number of active sites and the quantum yield. In recent years, Chen et al. (2014) used organic molecule 2-azidimidazole as a precursor to synthesize N-dots with the nitrogen content as high as 34.5%. Its particle size was less than 10 nm and had excellent optical properties with high fluorescence quantum yield, no photobleaching, adjustable emission spectrum and good biocompatibility. Tang et al. purposed the rapid preparation of N-dots and developed application in fluorescence, Raman, etc. (Tang et al., 2017; Lin et al., 2018). Interestingly, Zheng et al. (2017) prepared novel N-dots with nitrogen content up to 57% using 5-aminotetrazole as a precursor by a one-step hydrothermal method, and the N-dots had excellent performance of enhancing a chemiluminescent signal. N-dots as a new member of the QDs family with excellent optical properties and satisfactory biocompatibility have broad application prospects in the fields of point-of-care analysis and bioimaging.

ECL is an electrogenerated chemiluminescence technology, which integrates the distinct advantages of electrochemistry and spectroscopy. ECL not only has low background noise without auto-fluorescence and scattered light, but also can be regulated with high reproducibility and accuracy. Therefore, ECL analytical methods have attracted much considerable attention in the bioanalysis and clinical diagnostics. From 2002, QDs have been employed into the ECL sensing research due to the good stability, functional flexibility, ideal optical properties, and low cost. Some ECL sensing mode, such as ECL-RET (Wang et al., 2018) and SPC-ECL (Liu et al., 2018), have been applied in the bioanalysis. However, there are several challenges in the development of QDs-based ECL sensors. The intrinsic issues about the low ECL efficiency, the unclear ECL mechanism, and the exploration of new ECL sensing mode are still unsolved.

In this work, as shown in Fig. 1, we applied an effective coreactant modifier-based amplified ECL sensing mode with N-dots/galactose oxidase (GAox) for accurate detection of GA. We modified N-dots and GAox with chitosan on the glassy carbon electrode (GCE). GAox can catalyze the oxidation of GA and produce hydrogen peroxide. Due to the low ECL efficiency of N-dots with hydrogen peroxide, the product of hydrogen peroxide can not be detected intuitively. Therefore, we applied coreactant modifier-based amplified ECL system to greatly enhance emission signal. With coreactant modifier-based amplified ECL system, the ECL emission of N-dots increased ca. 40- and 7.7-times intensity over that of H_2O_2 or $K_2S_2O_8$ as an individual coreactant. Therefore, the application of the coreactant modifier-sensing mode can amplify the ECL signal and increase accuracy and sensitivity for the GA detection. Moreover, the change of the ECL signal can be easily observed with a smartphone camera and made it possible for practical point-of-care test of GA.

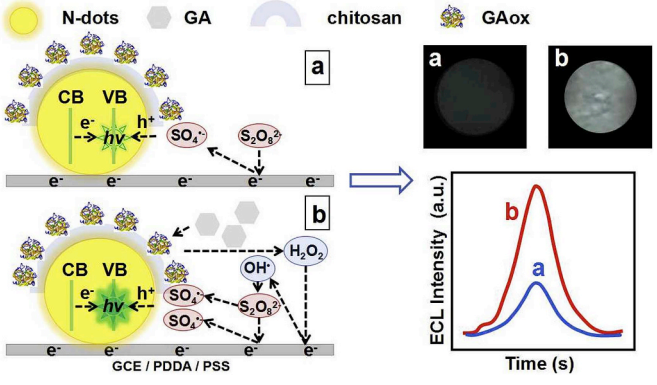

Fig. 1. Schematic illustration of the N-dots/GAox sensor.

2. Experimental section

2.1. Reagents and apparatus

All reagents were of analytical grade and used directly without further purification. 2-aminoimidazolium sulfate, hydrochloric acid, sodium nitrite, sodium azide, sodium hydrogencarbonate, ethyl acetate, sodium sulfate and aqueous ammonia were purchased from Beijing Chemical Works. GAox was purchased from Sigma. Poly dimethyl diallyl ammonium chloride, poly (sodium-p-styrene sulfonate), chitosan, GA, potassium persulfate, hydrogen peroxide, sodium hydrogen phosphate, sodium dihydrogen phosphate, sodium phosphate, glucose, fructose, glycine, arginine, tryptophan, threonine and aspartic acid were purchased from Sangon Biotech Co., Ltd (Shanghai, China). All reagents were prepared using ultrapure water with a resistivity of greater than 18 MΩ cm^{-1}. Human serum was obtained as a gift from the school hospital, Jilin University. All experiments were carried out at room temperature.

Photoluminescence (PL) spectra measurements were performed on a Shimadzu RF-5301 PC spectrofluorophotometer (Shimadzu Co., Kyoto, Japan). Transmission electron microscopy (TEM) images were obtained with a Hitachi electron microscope operating at a 200 kV acceleration voltage. The ultraviolet-visible (UV-vis) absorption spectra were acquired on a Varian GBC Cintra 10e UV-vis spectrometer with a 1 cm quart cell. Fourier transform infrared spectrometry (FT-IR) was conducted on a Thermo Nicolet 360 FTIR spectrometer using KBr pellets. All pH measurements were taken with a PHS-3C pH meter (Tuopu Co., Hangzhou, China). The electrochemical data were acquired with a CHI 660B electrochemical workstation with a three-electrode system. ECL signals were acquired by a BPCL ultraweak luminescence instrument. The voltage of the photomultiplier tube (PMT) was set at 900 V during the whole process. A conventional three-electrode system was used in this system. A glassy carbon electrode was used as the working electrode. A platinum wire was employed as the counter electrode and an Ag/AgCl (saturated KCl) electrode as the reference electrode.

2.2. Synthesis of N-dots

N-dots were synthesized according to the previous reports (Tang et al., 2017). At first, 2-aminoimidazole sulfate (0.825 g) was dissolved in hydrochloric acid (5.0 mol L^{-1}, 5 mL). Then the sodium nitrite solution (0.435 g sodium nitrite dissolved in 8 mL ultrapure water) and NaN_3 solution (0.408 g NaN_3 dissolved in 3 mL ultrapure water) were added slowly into the mixture solution under stirring at 0 °C. The mixture solution was stirred at room temperature for about 20 h to obtain the precursor (2-azidoimidazole). After the reaction was completed, pH of the reaction mixture was adjusted to 7.5 by adding saturated sodium bicarbonate solution. The yellow synthesized precursor was extracted from the mixture with ethyl acetate, and dried via anhydrous Na_2SO_4, and rotary evaporated. At last, under the microwave-assisted hydrothermal condition (120 °C, 8 min), 0.05 g 2-azidoimidazole was dissolved in 10 mL aqueous ammonia to synthesize N-dots. To remove excess precursor, the N-dots solution were centrifuged at 12000 rpm for 20 min and washed two times. The red-brown product

was dried and dispersed in 15 mL ultrapure water under ultrasound.

2.3. ECL detection

For ECL detection, the bare GCE was polished with 1.0 and 0.05 μm α-Al_2O_3 powder on a polished cloth, then ultrasonically cleaned in ethanol and ultrapure water to obtain a mirror-like surface. The cleaned electrode was soaked in 0.5% PDDA solution and 0.5% PSS solution for 5 min, respectively. 4 μL of N-dots solution was dropped on pretreated GCE surface and dried at room temperature, then 6 μL of 0.2% chitosan solution was dropped and completely dried. Next, 10 μL of 4 mg mL^{-1} GAox solution was dropped onto the electrode surface and dried. The modified electrode was immersed in different concentrations of GA solution and PBS (pH 7.4) at 37 °C for 40 min. After the reaction was completed, potassium persulfate solution was added (1 mM final) to record the ECL intensity. The ECL signal was collected under cyclic voltammetry from 0 to −2.5 V. Human serum was obtained from the school hospital of Jilin University. Samples were centrifuged at 10 000 rpm for 10 min to separate. A 1.0 mL aliquot of the serum sample was mixed with 1.5 mL of acetonitrile. After shaking, the solution was centrifuged at 10 000 rpm for 10 min. The supernatant was adjusted to pH 7.4 with phosphate buffer solution. Different concentrations of GA were added to the diluted serum samples to prepare the spiked samples.

2.4. Visual detection

The visual detection employed a piece of 6 cm × 5 cm FTO glass and a HUAWEI smartphone. The pictures were obtained with a CHI 660B electrochemical workstation. In the three-electrode system, FTO glass acted as the working electrode. The excitation voltage ranged from −2.5 V to 0 V. The images of the ECL detection were displayed by a CMOS sensor chip (1920 × 1080 pixels) embedded on the smartphone camera. In order to avoid the interference of environment light on the visual detection process, the ECL detection process was carried out with the assistance of a black shading box, which improved convenience to point-of-care test.

3. Results and discussion

3.1. Characterization of N-dots

Fig. 2 showed uniform size and satisfactory dispersion of N-dots with a diameter of 3 nm and clearly ordered lattice fringes of 0.17 nm, which revealed good crystallization of N-dots. The surface composition of N-dots was characterized by XPS. As shown in Fig. S1, we observed that N-dots were rich in nitrogen. The peaks at 288.7 eV and 284.6 eV were corresponding to C=O and C=C, the peak at 399.25 eV was corresponding to NH_2, the peak at 532.24 eV was corresponding to C-O. The Fourier transform infrared (FTIR) spectrum in Fig. S2 (A) also indicated the surface functional groups of N-dots. The stretching vibration peak of O-H and N-H were at 3750-3000 cm^{-1} and the stretching vibration peaks of C-N and C-O-C were at 1475-1000 cm^{-1}. Other characteristic peaks were observed at 1680 cm^{-1} and 1510 cm^{-1}, which represented C=O and C=C/C=N, respectively. Fig. S2 (B) showed the UV spectrum of N-dots. We observed strong absorption of N-dots at 423 nm, indicating the transition of n electron or π electron to π* excited state. As shown in Fig. S3, the emission peak position of N-dots changed with increase of excitation wavelength from 320 nm to 400 nm. It demonstrated excitation wavelength dependence of N-dots. Compared to the PL emission peak, as shown in Fig. S4, due to surface states and surface defects of N-dots, significant red shift of the ECL emission peak was observed. The effect of surface states for ECL charge injection was opposite to the photo injection. Enough energy produced from the electron transfer on surface of N-dots generate ECL emission light. Therefore, an obviously red shift of ECL peak from the photoluminescence peak formed with narrower band gaps than the core of N-dots surface state. We can find similar situations from the following references (Sun et al., 2009; Liu et al., 2018). We measured the quantum yield of the N-dots to be 40% (quinine sulfate 54%) and ECL efficiency of N-dots to be 4.6% (Ru $(bpy)_3^{2+}$ 5%).

3.2. Coreactant modifier-based amplified ECL mechanism

In the process of coreactant promoting ECL emission (Poznyak et al., 2004; Li et al., 2010; Kang et al., 2007), $S_2O_8^{2-}$ was reduced firstly to a strong oxidant ($SO_4^{\bullet-}$) with sufficiently negative electrode potential as coreactant. The formed $SO_4^{\bullet-}$ injected holes into the valence band of luminophore. Then the electrons from the conduction band combined with the holes, resulting in the excited-state species of luminophore and emitted light. The detailed N-dots/$K_2S_2O_8$ ECL mechanism can can be explained as follows:

$$S_2O_8^{2-} + e^- \rightarrow SO_4^{\bullet-} + SO_4^{2-} \quad (1)$$

$$SO_4^{\bullet-} + \text{N-dots} + e^- \rightarrow \text{N-dots}^* + SO_4^{2-} \quad (2)$$

$$\text{N- dots}^* \rightarrow \text{N-dots} + h\nu \quad (3)$$

As shown in Fig. 3, we observed significant enhancing ECL emission of N-dots/$K_2S_2O_8$ by H_2O_2 as coreactant modifier. The coreactant modifier can generate ca. 40- and 7.7-times intensity over that of H_2O_2

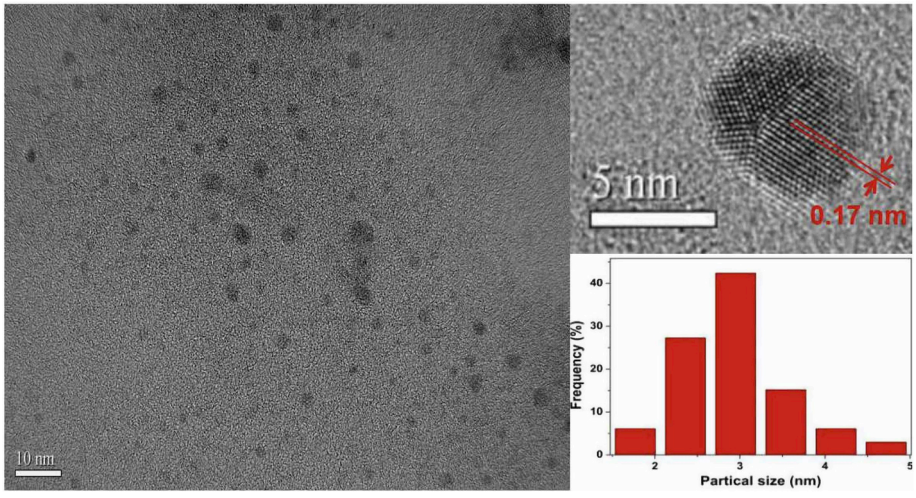

Fig. 2. HRTEM image of the N-dots.

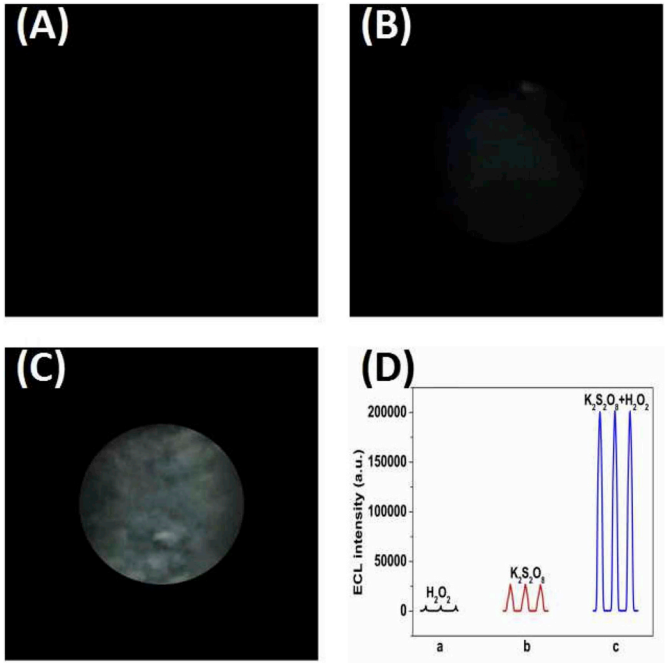

Fig. 3. Digital images of the ECL emission of N-dots in 0.01 M PBS (pH 7.4) containing (A) 10^{-2} M H_2O_2, (B) 10^{-3} M $K_2S_2O_8$, (C) 10^{-2} M H_2O_2 and 10^{-3} M $K_2S_2O_8$, (D) The ECL curves of N-dots in 0.01 M PBS (pH 7.4) containing (a) 10^{-2} M H_2O_2, (b) 10^{-3} M $K_2S_2O_8$, (c) 10^{-2} M H_2O_2 and 10^{-3} M $K_2S_2O_8$.

or $K_2S_2O_8$ as an individual coreactant, respectively. Although H_2O_2 can also be used as coreactant in some ECL system, it was hard to generate satisfactory electroluminescence effect, which indicated that H_2O_2 did not work as an effective coreactant for N-dots ECL. Meanwhile, compared with the weak ECL emission produced by N-dots in $K_2S_2O_8$ or H_2O_2 as an individual coreactant, the obvious ECL image of N-dots with $K_2S_2O_8$ and H_2O_2 can be easily recorded by the smartphone COMS. Therefore, we can confirm the good effect of the coreactant modifier, which showed the satisfactory application of the coreactant modifier system in the detection of enzymes that can produce hydrogen peroxide and the possibility of direct observation of the signal changes.

As shown in Fig. S5, when H_2O_2 or $K_2S_2O_8$ acted as an individual coreactant, respectively, the potential of N-dots hardly changed, while the ECL signal in $K_2S_2O_8$ was stronger. In $K_2S_2O_8/H_2O_2$ system, the potential of N-dots changed from −2.5 V to −2.0 V, and the ECL signal of N-dots remarkably enhanced. This result indicated synergistic effect of $K_2S_2O_8$ and H_2O_2 in N-dots ECL emission (Dai et al., 2015). Meanwhile, compared with $OH^{\bullet}$, the oxidant $SO_4^{\bullet-}$ with a stronger oxidizing capacity acted as the leading role in the hole injection to valence band of N-dots with the assistance of $OH^{\bullet}$ produced from H_2O_2.

As shown in Fig. S4, the weak ECL peak of N-dots in H_2O_2 was different from that in $K_2S_2O_8$ solution and $K_2S_2O_8/H_2O_2$ system, indicating the different luminescence mechanisms of N-dots in H_2O_2. In H_2O_2, the peak at around 555 nm was observed due to the excessive $OH^{\bullet}$, which can be attributed to the emission of $^1(O_2)_2$* in the N-dots/H_2O_2 system (Ma et al., 2015). Then in $K_2S_2O_8$ solution and $K_2S_2O_8/H_2O_2$ system, the significantly enhanced emission peak at 535 nm was attributed to the radiative deactivation of N-dots*. The disappearance of the peak at 555 nm indicated almost no emission of $^1(O_2)_2$* in $K_2S_2O_8/H_2O_2$ system. As for the peaks in $K_2S_2O_8$ solution and $K_2S_2O_8/H_2O_2$ system, the position of the peaks at 535 nm were unchanged, but the ECL intensity in $K_2S_2O_8/H_2O_2$ system was much stronger than that in $K_2S_2O_8$ solution. In summary, we proved that in $K_2S_2O_8/H_2O_2$ system, $K_2S_2O_8$ acted as a leading role in the process of coreactant promoting luminescence of N-dots, and the effect of H_2O_2 was to assist $K_2S_2O_8$ to generate more strong oxidant ($SO_4^{\bullet-}$) for stronger electroluminescence. This conclusion was consistent with the previous reports. According to previous report (Bartlett and Cotman, 1949; Ye et al., 2009), $OH^{\bullet}$ can induce decomposition of $K_2S_2O_8$ to produce more $SO_4^{\bullet-}$ as follows:

$$OH^{\bullet} + S_2O_8^{2-} \rightarrow SO_4^{\bullet-} + HSO_4^{-} + 1/2\ O_2 \quad (4)$$

Therefore, as shown in Fig. S6, the $OH^{\bullet}$ produced by H_2O_2 promoted the generation of $SO_4^{\bullet-}$ by $K_2S_2O_8$. As the concentration of $SO_4^{\bullet-}$ injecting holes into the N-dots increased, the number of positive N-dots increased, resulting in higher stability and stronger ECL signals.

In summary, H_2O_2 worked as coreactant modifier to promote the generation of strong oxidant ($SO_4^{\bullet-}$) by $K_2S_2O_8$. The coreactant modifier-based amplified ECL mechanism was as follows:

$$S_2O_8^{2-} + e^- \rightarrow SO_4^{\bullet-} + SO_4^{2-} \quad (5)$$

$$H_2O_2 + e^- \rightarrow OH^{\bullet} + OH^- \quad (6)$$

$$OH^{\bullet} + S_2O_8^{2-} \rightarrow SO_4^{\bullet-} + HSO_4^{-} + 1/2\ O_2 \quad (7)$$

$$SO_4^{\bullet-} + \text{N-dots} + e^- \rightarrow \text{N-dots*} + SO_4^{2-} \quad (8)$$

$$\text{N-dots*} \rightarrow \text{N-dots} + h\nu \quad (9)$$

We investigated the effect of concentrations of $K_2S_2O_8$ and H_2O_2 on the ECL intensity of N-dots. We can observed from Fig. S6 that the ECL intensity of N-dots increased with the increasing concentration of $K_2S_2O_8$. When the concentration of $K_2S_2O_8$ was constant, the increase of the concentration of H_2O_2 also signified more synergistic effect, which promoted the enhancement of ECL signal of N-dots. However, when H_2O_2 was excessive to 1 M, $SO_4^{\bullet-}$ can be decomposed by $OH^{\bullet}$ to reduce the ECL signal (Bartlett and Cotman, 1949). More data have listed in Table S1.

3.3. GA detection

The impedance changes on the modified electrode from electrochemical impedance spectroscopy (EIS) were shown in Fig. S7 (A). The larger semicircle diameter indicated the larger charge transfer resistance (Rct) values of the modified electrode. The bare GCE showed a mass diffusion limiting process. After modifying PDDA/PSS/N-dots, the Rct increased to 375.2 Ω. Then there existed obvious increase at 602.4 Ω after chitosan and GAox was modified. It indicated that N-dots/GAox sensor was developed successfully. In addition, with the assembly of N-dots, chitosan and GAox on the electrode, the current in the cyclic voltammetry curve (Fig. S7 (B)) gradually decreased, which also confirmed the realization of layer modification. The stability research was shown in Fig. S7 (C). The stability of sensor was studied by measurements (n = 10) in PBS (pH = 7.4) and 10^{-3} mol L^{-1} $K_2S_2O_8$ solution. The relative standard deviations (RSD) of the sensor was 2.04%. This confirmed the brilliant stability of the sensor. In order to obtain a wider linear range and more intuitive changes in the subsequent detection work, we chose the most appropriate concentration of $K_2S_2O_8$. From Fig. S6, when the concentration of $K_2S_2O_8$ was 10^{-3} M, H_2O_2 as coreactant modifier maximized ECL signal amplification of N-dots (40 times) (as shown in Fig. S8). Therefore, we designed to detect the amplified N-dots ECL signal from hydrogen peroxide produced by GAox for sensitive detection of GA. When GA was added in the sensing system, GAox catalyzed decomposition of GA and produced H_2O_2. H_2O_2 worked as coreactant modifier to promote the generation of strong oxidant ($SO_4^{\bullet-}$). As a result, the ECL intensity of N-dots increased with increasing GA concentration in Fig. 4. The linear equation between the logarithm of GA concentration and the ECL intensity was I = 5895.9 log [GA] + 73035 with an LOD of 0.16 μmol L^{-1}. The correlation coefficient was 0.97. This linear range covered the clinical diagnostic limit, which proved the actual significance of the proposed sensor. More importantly, due to the application of the coreactant modifier-based amplified ECL system, we achieved significant amplification and digital

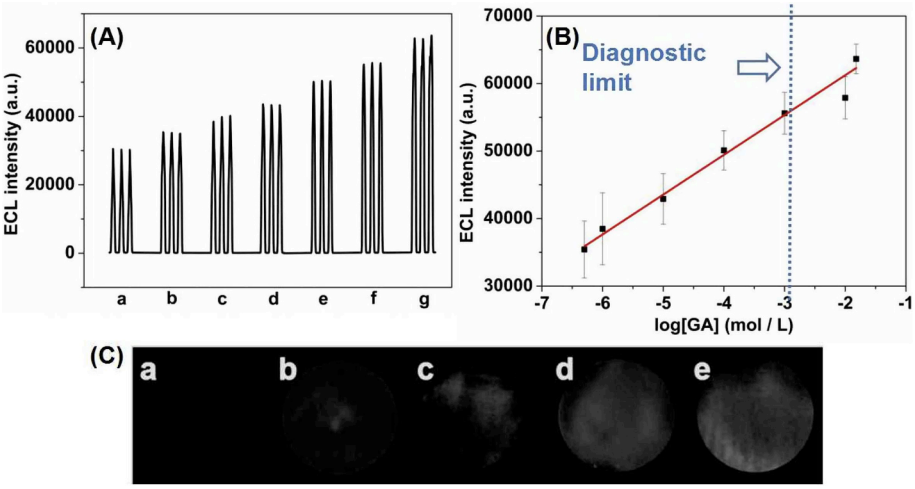

Fig. 4. (A) ECL trace of N-dots/GAox sensor of different concentrations of GA (from a to g: 5×10^{-7}, 10^{-6}, 10^{-5}, 10^{-4}, 10^{-3}, 10^{-2}, 1.5×10^{-2} M). (B) Calibration curve for quantification of GA. (C) Digital images of the ECL emission of the sensor in 0.01 M PBS (pH 7.4) containing 10^{-3} M $K_2S_2O_8$ and 5×10^{-7}, 10^{-4}, 10^{-3}, 10^{-2}, 1.5×10^{-2} M GA (from a to e).

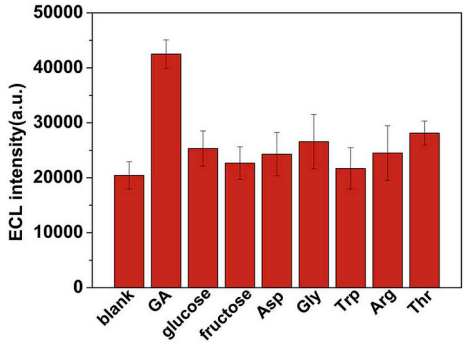

Fig. 5. The effect of different reaction substances on ECL intensity of N-dots/GAox sensor.

Table 1
Results for detection of GA in the real samples.

	Add (mol L^{-1})	Found (mol L^{-1})	Recovery (%)	RSD (%, n = 3)
1	10^{-6}	1.04×10^{-6}	104	4.23
2	10^{-4}	0.98×10^{-4}	98	2.04
3	10^{-2}	1.03×10^{-2}	103	3.19

imaging of the N-dots ECL signal. In the ECL digital images, it was obvious that the ECL intensity changed significantly with different GA concentration. Visualization of the ECL signal made the sensing mode more feasible in clinical applications. As shown in Fig. 5, we also evaluated the selectivity of the sensor. The sensor showed superior selectivity in 20-fold concentrations of glucose and fructose and 15-fold glycine, arginine, tryptophan, threonine and aspartic acid. Finally, the method was applied to detect human serum with a standard addition method. As shown in Table 1, the range of recoveries was from 98% to 104% and the RSD was less than 4.23%. The results indicated the reliability and accuracy of the GA sensor in actual application. Most importantly, as shown in Table S2, compared to other methods for detecting GA, our method was simple and effective with low detection limit and visual detection.

4. Conclusion

In this work, we have developed a coreactant modifier-based sensing mode to amplify N-dots ECL intensity. On the modified electrode with N-dots and GAox, H_2O_2 produced by the interaction of GAox with GA worked as coreactant modifier to promote the generation of strong oxidant of $K_2S_2O_8$ for N-dots ECL. As expected, ECL intensity increased ca. 40- and 7.7-times than that in H_2O_2 or $K_2S_2O_8$ as an individual coreactant, respectively. The coreactant modifier-based ECL sensor not only overcame the limitation of the low ECL efficiency of QDs, but also greatly improved the accuracy and sensitivity of GA detection. The proposed biosensor accurately quantified GA from 0.5 μmol L^{-1} to 15 mmol L^{-1} with a limit of detection of 0.16 μmol L^{-1}. More importantly, the true-color ECL signal of the coreactant modifier-based GA sensor can be easily imaged by a smartphone, which has great potential in the point-of-care test. Because how to realize high-resolution digital ECL imaging is still concerned, we will devote to the exploration about the sensitive and miniaturized handhelds for ECL detection and imaging in the future work.

CRediT authorship contribution statement

Yixin Nie: Conceptualization, Data curation, Formal analysis, Investigation, Methodology, Project administration, Writing - original draft, Writing - review & editing. **Yang Liu:** Investigation. **Qian Zhang:** Investigation. **Xingguang Su:** Investigation. **Qiang Ma:** Investigation.

Acknowledgements

The authors gratefully acknowledge financial support from the Youth Science Fund of Jilin Province (20140520081JH) and the "Thirteenth Five Year" Project of the Science and Technology Research in the Education Department of Jilin Province, China.

Appendix A. Supplementary data

Supplementary data to this article can be found online at https://doi.org/10.1016/j.bios.2019.111318.

References

Alivisatos, A.P., 1996. Science 271, 933–937.
Bagalkot, V., Zhang, L., Levy-Nissenbaum, E., Jon, S.Y., Kantoff, P.W., Langerand, R., Farokhzad, O.C., 2007. Nano Lett. 7, 3065–3070.
Baker, S.N., Baker, G.A., 2010. Angew. Chem. Int. Ed. 49, 6726–6744.
Bartlett, P.D., Cotman Jr., J.D., 1949. J. Am. Chem. Soc. 71, 1419–1422.
Brahim, S.I., Maharajh, D., Narinesingh, D., Guiseppi-Elie, A., 2002. Anal. Lett. 35, 797–812.
Cao, L., Wang, X., Meziani, M.J., Lu, F., Wang, H., Luo, P., Lin, Y., Harruff, B.A., Veca, L.M., Murray, D., Xie, S., Sun, Y., 2007. J. Am. Chem. Soc. 129, 11318–11319.
Chen, X., Jin, Q., Wu, L., Tang, X., 2014. Angew. Chem. Int. Ed. 53, 12542–12547.
Dai, P., Yu, T., Shi, H., Xu, J., Chen, H., 2015. Anal. Chem. 87, 12372–12379.
Ding, Z., Quinn, B.M., Haram, S.K., Pell, L.E., Korgel, B.A., Bard, A.J., 2002. Science 296, 1293–1297.
Easley, C.J., Jin, L.J., Presto Elgstoen, K.B., Jellum, E., Landers, J.P., Ferrance, J.P., 2003. J. Chromatogr. 1004, 29–37.
Englund, D., Fattal, D., Waks, E., Solomon, G., Zhang, B., Nakaoka, T., Arakawa, Y.,

Yamamoto, Y., Vuckovic, J., 2005. Phys. Rev. Lett. 95, 13904.
Fan, X., Feng, Y., Su, Y., Zhang, L., Lv, Y., 2015. RSC Adv. 5, 55158–55164.
Gao, X., Cui, Y., Levenson, R.M., Chung, L.W., Nie, S., 2004. Nat. Biotechnol. 22, 969–976.
Garcia-Carmona, L., Rojas, D., Gonzalez, M.C., Escarpa, A., 2016. Analyst 141, 6002–6007.
Kang, J., Wei, H., Guo, W., Wang, E., 2007. Commun 9, 465–468.
Larson, D.R., Zipfel, W.R., Williams, R.M., Clark, S.W., Bruchei, M.P., Wıˆse, F.W., Webb, W.W., 2003. Science 300, 1434–1436.
Lee, K.N., Lee, Y., Son, Y., 2011. Electroanalysis 23, 2125–2130.
Li, J., Yang, L., Luo, S., Chen, B., Li, J., Lin, H., Cai, Q., Yao, S., 2010. Anal. Chem. 82, 7357–7361.
Lin, L., Xu, Y., Zhang, S., Ross, I.M., Ongand, A.C., Allwood, D.A., 2014. Small 10, 60–65.
Lin, Z., Yang, J., Tang, Z., Li, G., Hu, Y., 2018. Talanta 178, 515–521.
Liu, Y., Chen, X., Wang, M., Ma, Q., 2018. Green Chem. 20, 5520–5527.
Ma, M., Zhang, X., Zhuo, Y., Chai, Y., Yuan, R., 2015. Nanoscale 7, 2085–2092.
Manowitz, P., Stoecker, P.W., Yacynych, A.M., 1995. Biosens. Bioelectron. 10, 359–370.
Medintz, I.L., Uyeda, H.T., Goldman, E.R., Mattoussi, H., 2005. Nat. Mater. 14, 435–446.
Michalet, X., Pinaud, F.F., Bentolila, L.A., Tsay, J.M., Doode, S., Li, J., Sundaresan, G., Wu, A., Gambhir, S.S., Weiss, S., 2005. Science 307, 538–544.
Nishimura, Y., Tajima, G., Dwi Bahagia, A., Sakamoto, A., Ono, H., Sakura, N., Naito, N.K., Hamakawa, M., Yosh, C., Kubota, M., Kobayashi, K., Saheki, T.J., 2004. Inherit. Metab. Dis. 27, 11–18.
Pan, D., Zhang, J., Li, Z., Wu, M., 2010. Adv. Mater. 22, 734–738.
Ponomarenko, L.A., Schedin, F., Katsnelson, M.I., Yang, R., Hill, E.W., Novoselov, K.S., Geim, A.K., 2008. Science 320, 356–358.
Poznyak, S.K., Talapin, D.V., Shevchenko, E.V., Weller, H., 2004. Nano Lett. 4, 693–698.
Sasaki, S., Franceschi, S.D., Elzerman, J.M., Wiel, W.G., Eto, M., Tarucha, S., Kouwenhoven, L.P., 2000. Nature 405, 764–767.
Shen, J., Zhu, Y., Yang, X., Li, C., 2012. Chem. Commun. 48, 3686–3699.
Stoecker, P.W., Manowitz, P., Yacynych, A.M., 1995. Biosens. Bioelectron. 10, 359–370.
Sun, Y., Zhou, B., Lin, Y., Wang, W., Fernando, K.A., Pathak, P., Meziani, M.J., Harruff, B.A., Wang, X., Wang, H., Luo, P., Yang, H., Kose, M.E., Chen, B., Veca, L.M., Xie, S., 2006. J. Am. Chem. Soc. 128, 7756–7757.
Sun, L., Bao, L., Hyun, B.R., Bartnik, A.C., Zhong, Y.W., 2009. Nano Lett. 9, 789–793.
Sun, M., Deng, D., Zhang, K., Lu, T., Su, Y., Lv, Y., 2016. Chem.Commun. 52, 11259–11262.
Tang, Y., Song, H., Su, Y., Lv, Y., 2013. Anal. Chem. 85, 11876–11884.
Tang, Y., Su, Y., Yang, N., Zhang, L., Lv, Y., 2014. Anal. Chem. 86, 4528–4535.
Tang, Z., Lin, Z., Li, G., Hu, Y., 2017. Anal. Chem. 89, 4238–4245.
Taylor, P.J., Kmetec, E., Johnson, J.M., 1977. Anal. Chem. 49, 789–794.
Tk´c1, J., Gemeiner, P., Šturd´k, E., 1999. Biotechnol. Tech. 13, 931–936.
Wang, H., Chai, Y., Li, H., Yuan, R., 2018. Biosens. Bioelectron. 100, 35–40.
Ye, M., Chen, Z., Liu, X., Ben, Y., Shen, J., 2009. J. Hazard Mater. 167, 1021–1027.
Yeh, T.F., Teng, C.Y., Chen, S.J., Teng, H.S., 2014. Adv. Mater. 26, 3297–3303.
Zhang, Z., Li, J., Wang, X., Shen, D., Chen, L., 2015. ACS Appl. Mater. Interfaces 7, 9118–9127.
Zheng, Y., Zhang, D., Shah, S.N.A., Li, H., Lin, J., 2017. Chem. Commun. 53, 5657–5660.
Zhu, S., Meng, Q., Wang, L., Zhang, J., Song, Y., Jin, H., Zhang, K., Sun, H., Wang, H., Yang, B., 2013. Angew. Chem. Int. Ed. 52, 3953–3957.
Zrazhevskiy, P., Sena, M., Gao, X., 2010. Chem. Soc. Rev. 39, 4326–4354.